ELSEVIER

Remote Sensing of Environment 82 (2002) 376–388

Remote Sensing of Environment

www.elsevier.com/locate/rse

Determining land surface fractional cover from NDVI and rainfall time series for a savanna ecosystem

Todd M. Scanlon *, John D. Albertson [1], Kelly K. Caylor, Chris A. Williams

Department of Environmental Sciences, Clark Hall, University of Virginia, Charlottesville, VA 22903, USA

Received 25 October 2001; received in revised form 1 April 2002; accepted 6 April 2002

Abstract

Savanna ecosystems are water limited and responsive to rainfall on short time scales, characteristics that can be exploited to estimate fractional cover of trees, grass, and bare soil over large-scale areas from synthesis of remote sensing and rainfall measurements. A method is presented to estimate fractional cover based upon the differing ways in which grasses and trees respond to rainfall, and implementation of this method is demonstrated along the Kalahari Transect (KT), an aridity gradient in southern Africa. Seasonally averaged normalized difference vegetation index (NDVI) and the sensitivity of the NDVI to interannual variations in wet season rainfall are used as state-space variables in a linear unmixing model. End members for this analysis were determined on the basis of best fit to the observed data. The realized end members were consistent with the qualitative characteristics of trees (high NDVI, low sensitivity of NDVI to interannual variations in rainfall), bare soil (low NDVI, low sensitivity), and the transient grass/ bare soil area (moderate NDVI, high sensitivity). Observed sensitivity of NDVI to rainfall was measured as the relationship between wet season NDVI and normalized rainfall over a 16-year period (1983–1998). The unmixing model yields a north-to-south decrease in tree fractional cover that corresponds to the decrease in mean wet season precipitation from 1600 to 300 mm along the KT (R^2=.87). The fractional tree cover results compare favorably with available ground-based observations. The potential extent of grass cover is limited by the dominance of trees on the northern end of the transect, peaks at the location with approximately 450 mm of mean wet season rainfall, and is limited by rainfall in the arid southern portion of the transect. With mean NDVI for grass inferred from the data, yearly estimates of tree, grass, and bare soil fractional cover can be derived. These annual estimates, which are difficult to obtain from traditional unmixing procedures, are important parameters in fuel load and land–atmosphere exchange models. No calibration or training sets were required for this analysis, and this method has the additional capability to predict fractional-cover components for future rainfall scenarios.

1. Introduction

Savanna ecosystems are characterized by the coexistence of woody and herbaceous vegetation, the relative abundance of which defines important aspects of the biome such as fuel biomass and combustion factors for fire (Hoffa, Ward, Hao, Susott, & Wakimoto, 1999; Shea et al., 1996), fauna habitat (Doergeloh, 2000; Dean, Milton, & Jeltsch, 1999), nutrient cycling (Belsky, 1994; Frost, 1984), and resources for human subsistence. Frequently stressed and sensitive to change (Guenther, Zimmerman, Greenberg, Scholes, & Scholes, 1996), savanna ecosystems are responsive to climate variability on relatively short time scales. Water is the main driving force in shaping the vegetation composition and distribution for these semiarid systems (Rodriguez-Iturbe, D'Odorico, Porporato, & Ridolfi, 1999a, 1999b; Smit & Rethman, 2000). The dynamic quality of the vegetation with respect to precipitation forcing can be monitored over a large spatial area with the aid of remote sensing and inferences about rainfall–vegetation processes in these savanna ecosystems can thus be developed. With the added benefit of sufficient temporal coverage, remote sensing can now be used to make predictions of the earth's vegetation dynamics with respect to future climate scenarios based upon analysis of these past observations. In this paper, we merge ground-based rainfall measurements with remotely sensed data to infer the surface cover components of a savanna system from the rainfall response properties of the individual components.

* Corresponding author. Tel.: +1-434-924-0555; fax: +1-434-982-2137.
E-mail address: tms2v@virginia.edu (T.M. Scanlon).
[1] Now at Department of Civil and Environmental Engineering, Box 90287, Duke University, Durham, NC 27708-0287, USA.

0034-4257/02/$ - see front matter © 2002 Published by Elsevier Science Inc.
PII: S0034-4257(02)00054-8

Several factors make the Kalahari Transect (KT) in southern Africa an ideal location for assessment of this concept. The KT is one in the global set of International Geosphere–Biosphere Programme (IGBP) transects (Koch, Scholes, Steffen, Vitousek, & Walker, 1995), spanning a north–south aridity gradient from Angola and Zambia, through Botswana, and into South Africa (Thomas & Shaw, 1993). A homogeneous aeolian sand formation underlies a large portion of the transect, providing a relatively uniform background reflectance. Savanna vegetation is optimal for the use of remote sensing (Palmer & van Rooyen, 1998) because, unlike with closed canopies, spectral saturation is not a problem, thereby enabling the recognition by a remote sensor of subtle differences in the true amount of green biomass. Previous applications of remote sensing in Africa have focused on the link between water availability and vegetation biomass (e.g., Farrar, Nicholson, & Lare, 1994; Fuller & Prince, 1996; Nicholson & Farrar, 1994; Richard & Poccard, 1998). In southern Africa, there is observed to be a strong correspondence between the mean climatic distribution of precipitation and green biomass, as measured by mean annual normalized difference vegetation index (NDVI) (Goward & Prince, 1995), yet on shorter time scales the interannual variability in precipitation does not, in general, result in much variability in NDVI (Fuller, 1994). The exception to this was found to be in ''marginal zones'' (Goward & Prince, 1995), areas bounded by high and low annual precipitation such as the middle region of the KT, where the vegetation appears to respond strongly to year-to-year precipitation variability. This raises the question: What factors associated with the vegetation in these marginal zones cause the NDVI to be more dynamic in its response to precipitation? We hypothesize here that relative mixture of trees and grasses plays a primary role in defining this observed phenomenon.

In terms of strategies for using water, grasses are considered to be intensive exploiters while trees and shrubs are extensive exploiters (Burgess, 1995). With dense, shallow root systems, grasses make use of water that is ephemerally available in the upper layer of the soil while trees, which have root systems that penetrate both the shallow and deeper soil layers, have a more persistent supply of soil water. Relative to trees, grasses exhibit a greater areal expansion of biomass in response to rainfall in savanna ecosystems. Short-term greening of trees is restricted in areal extent by the standing woody biomass. Additionally, the photosynthetic pathways associated with trees and grasses differ such that grasses, in general, are able to synthesize more carbon per unit of water loss via transpiration than are trees (Ehleringer & Monson, 1993). This was supported by flux measurements taken along the KT (Scanlon & Albertson, submitted). All these factors contribute to greater expected NDVI response to precipitation by grasses relative to trees. This is the distinguishing property of the vegetation components that will be used to detect and model the dynamic vegetation composition of the savanna ecosystem along the KT, with wider applicability to savannas in general.

Subpixel-scale information about land cover classification or composition has often been obtained from spectral ''unmixing'' analysis, a richly developed and active area in the remote sensing and photogrammetry literature. This analysis is based on the principle that a spatially coarse spectral signal is a weighted function of the spectral contributions from the smaller-scale (i.e., subpixel) individual components. Linear unmixing models (e.g., DeFries, Hansen, & Townshend, 2000; Settle & Drake, 1993; Smith, Johnston, & Adams, 1985) used to detect surface cover are by far the most common, and, although theoretically imperfect due to the omission of the effect of multiple scattering between cover types (Myneni, Maggion, & Jaquinta, 1995; Roberts, Smith, & Adams, 1993), the errors associated with the linear assumptions have been found to be relatively minor (Kerdiles & Grondona, 1995). The output from the spectral unmixing applications generally falls into two categories: land cover classification types (i.e., forest, grassland, urban, etc.) or fractional-cover components (i.e., tree, grass, bare soil). A typical approach for determining either product, as outlined in DeFries et al. (2000), first involves the generation of numerous metrics from the multiple spectral bands (channels) that are present on remote sensing instruments. Often, the phenology of the vegetation is captured by selecting metrics that are related to the within-year variability measured by particular channels or combinations of channels. Next, the number of metrics is reduced to a smaller number of variables for use in the unmixing model by performing linear discriminant analysis. This procedure weights the metrics by maximizing the ratio of class means to within-class variance, thereby enabling maximum spectral separation between the cover types. Training sets, or spectral information from preclassified cover types, can then be used to define the spectral end members for the ''pure'' cover types for use in the unmixing model. Another way that spectral end members can be selected based on the metrics is through the use of principle component analysis (Bateson & Curtiss, 1996; Smith et al., 1985; Van Der Meer & De Jong, 2000). Both of these methods rely fundamentally upon empirical relationships between the vegetation and the spectral reflectance to define the land surface cover.

In the method presented here for finding the fractional surface cover components, we use a 16-year time series of NOAA Advanced Very High Resolution Radiometer (AVHRR) data along with the relationship that is derived between rainfall and NDVI as a means for a process-based identification of the tree, grass, and bare soil cover components. As pointed out by DeFries et al. (2000), using a multiyear AVHRR record must be cautiously undertaken due to the artifacts that remain in the record as a result of factors such as changes in sensors (NOAA-7 to NOAA-9 to NOAA-11 to NOAA-14 satellites), the impacts of aerosols from volcanic eruptions, other uncorrected atmospheric effects, and drift in equatorial crossing time. These very real problems require recalibration of the spectral end members each year with traditional spectral unmixing applications.

The sensitivity of the unmixing results to the recalibrated end members can lead to inferred land cover changes that did not actually occur (DeFries et al., 2000). By using the long term mean values of NDVI and the regressed sensitivity of the NDVI to rainfall along the KT, the net effect is that our method is insensitive to shorter time scale variability in NDVI that is not tied to variations in rainfall. As a consequence, we are able to largely circumvent this aforementioned problem.

The objectives of this research are to (1) determine the mean NDVI and sensitivity of NDVI to rainfall related to the individual components of the surface cover (tree, grass, bare soil) along the KT, (2) incorporate these properties in a linear unmixing model to derive fractional cover, and (3) develop a method to predict fractional cover in response to various future rainfall scenarios.

2. Methods

2.1. Data

Monthly NDVI data at 8-km resolution along the KT were acquired from the NASA/NOAA-sponsored AVHRR Land Pathfinder data set (Agbu & James, 1994; James & Kalluri, 1994) for the years 1983–1998 in the area bounded by 12° to 26°S latitude and 20.4° to 24.7°E longitude. The north–south oriented swath of NDVI data has the dimensions of 196×61 pixels. The maximum NDVI value for each pixel during a given month was assigned as the monthly value in an effort to eliminate cloud cover contamination; the Pathfinder processing team also applied atmospheric corrections for Rayleigh scattering as well as solar zenith angle. The analysis presented here focuses on the interannual variability in the savanna vegetation, rather than the within-year vegetation phenology, and therefore the southern African wet season, in which the vegetation is at its peak state, is used to represent the annual time series. Hence, the monthly NDVI time series fields were condensed into 16 "wet season" fields, representative of the averages for the months January, February, and March of each year in the data set. In actuality, the wet season in this region begins in mid-October. However, in order to be consistent with Grist, Nicholson, and Mpolokang's (1997) findings in Botswana that NDVI is most highly correlated with the precipitation in the concurrent plus two preceding months, the early portion of the wet season was not factored into the wet season average.

Monthly rainfall data were linearly interpolated to the same spatial resolution as the NDVI data from a 0.5° gridded precipitation data set (New, Holme, & Jones, 1999). The original data were gathered from southern African meteorological stations, approximately 11 of which fall within the bounds of the KT area studied here (Hulme, 1992a), and were checked for quality control (Eischeid, Diaz, Bradley, & Jones, 1991; Hulme, 1992b). The wet season rainfall is taken as the total for the months of November through March, covering a time frame that precedes the wet season NDVI by 2 months. On average, 87% of the total yearly rainfall arrives during this 5-month period for stations along the KT.

2.2. NDVI unmixing method

The linear unmixing technique that is applied to the wet season data utilizes observed long-term relationships between NDVI and precipitation, and assumes minimal large-scale vegetation alterations or land conversion during the 16-year period of analysis. We classify the fractional cover for each 8×8-km area in this region into three broad categories:

- a portion of the land surface that always remains as bare soil, $x_{b,only}$;
- a portion of the fractional cover that is woody vegetation (trees or shrubs), x_t; and,
- a remaining portion that consists of bare soil and herbaceous vegetation (grasses or forbs) cover, $x_{g/b}$.

The temporally constant $x_{g/b}$ fractional area is comprised of the temporally variable bare soil and grass cover fractions, x_{btrans} and x_{gtrans}, respectively (Fig. 1), such that $x_{g/b}=x_{btrans}+x_{gtrans}$. Note that tree fractional cover, x_t, is defined by the vertically projected area of the tree canopies and can therefore contain underlying grasses.

The north–south aridity gradient of the KT provides an ideal one-dimensional construct for the analysis. In order to the cast the fractional-cover profile of the transect in one dimension, spatial averaging was performed in the east–west direction, roughly parallel with the isohyets. This spatial averaging is denoted by the "<.>" operator and is applied along each of the 196 latitudinal positions i. With three unknown fractional-cover components, three equations are

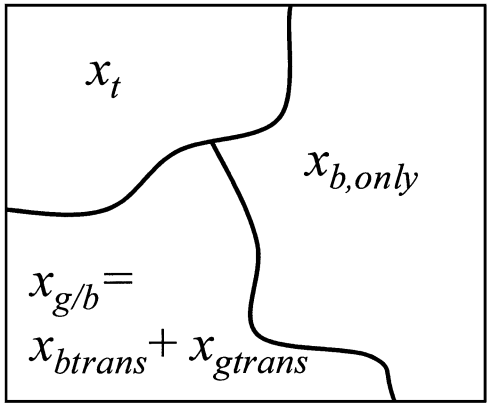

Fig. 1. Each pixel consists of three constant fractional covers that sum to one: tree cover (x_t), persistent bare soil cover ($x_{b,only}$), and transient grass/bare soil cover ($x_{g/b}$). During wet years, the grass fractional cover (x_{gtrans}) makes up the majority of $x_{g/b}$, while during dry years most of this area is bare soil (x_{btrans}).

needed to determine the fractional cover at each position i along the transect. The first equation stipulates that the total ground cover is made up entirely of the three temporally constant cover classifications:

$$\langle x_t(i)\rangle + \langle x_{b,only}(i)\rangle + \langle x_{g/b}(i)\rangle = 1. \quad (1)$$

The second equation states that the temporal mean of the observed wet season NDVI, $\overline{\alpha_{obs}}$, at each position i is equal to the sum of the mean NDVI associated with each component j, $\overline{\alpha_j}$ weighted by its fractional cover, $\langle x_j(i)\rangle$:

$$\overline{\alpha_t}\langle x_t(i)\rangle + \overline{\alpha_{b,only}}\langle x_{b,only}(i)\rangle + \overline{\alpha_{g/b}}\langle x_{g/b}(i)\rangle = \langle\overline{\alpha_{obs}}(i)\rangle. \quad (2)$$

Temporal averaging is denoted by the "—" operator. The values of $\overline{\alpha_{obs}}$, calculated from 48 months of wet season NDVI measurements, mask a number of temporally variable factors including vegetation cover, spectral interactions between components, relative brightness of the components (e.g., Hanan et al., 1991), as well as atmospheric- and sensor-related shifts. Therefore, $\overline{\alpha_{obs}}$ should be thought of as a general index of long-term greenness rather than being interpreted in terms of spectral composition of red and near-infrared reflectances. Implied from this is that the end members in Eq. (2), $\overline{\alpha_j}$, are not comprised of particular red and near-infrared reflectances either but instead represent a measure of long-term greenness for the individual components. The method by which $\overline{\alpha_j}$ are estimated, presented in the next section, exploits the observed, approximately linear mixing of the long-term greenness for use in the linear Eq. (2).

The third equation, making use of the linear property of the derivative, specifies that the overall sensitivity of the NDVI to rainfall, β_{obs}, is a function of the linearly weighted sensitivities of the individual cover types, β_j:

$$\beta_t\langle x_t(i)\rangle + \beta_{b,only}\langle x_{b,only}(i)\rangle + \beta_{g/b}\langle x_{g/b}(i)\rangle = \langle\beta_{obs}(i)\rangle. \quad (3)$$

The observed sensitivity of NDVI to rainfall can be found at each pixel by:

$$\beta_{obs} = \frac{d\alpha_{obs}}{d\hat{r}} \quad (4)$$

where $\hat{r}$ is the normalized wet season rainfall:

$$\hat{r} = (r - \bar{r})/\sigma_r. \quad (5)$$

Here, r is the rainfall for a given wet season and $\bar{r}$ and σ_r are the temporal mean and standard deviation of wet season rainfall, respectively. This normalization procedure is intended to prevent the extremely high or low rainfall values from disproportionately influencing the slopes of the NDVI–rainfall relationships.

In evaluating the sensitivity of the NDVI to rainfall, β_{obs}, the 16-year time series for both NDVI and precipitation at each pixel within the 196×61 grid were considered. Wet season NDVI was plotted as a function of normalized wet season rainfall, and the slope was determined from this relationship on a pixel-by-pixel basis. Significance of the linear fit relationship was evaluated on the basis of $P<.1$ for a one-tailed test. Only those correlations that were deemed significant on this basis were spatially averaged to generate the one-dimensional $\langle\beta_{obs}(i)\rangle$ along the KT.

2.3. End-member determination

This leaves the end-member values for the individual cover types, the coefficients $\overline{\alpha_j}$ in Eq. (2) and β_j in (3), as the remaining unknown parameters needed to perform the unmixing analysis. On a conceptual basis, relative estimates of mean NDVI and sensitivity of NDVI to rainfall for the individual components are evident from both color and lateral growth considerations. Trees are expected to have a high $\bar{\alpha}$ and a low β, the bare soil a low $\bar{\alpha}$ and low β, while the transient grass/bare soil area is expected to have a moderate $\bar{\alpha}$ and a high β. Pixels that contain more than one of these cover types display an average, weighted by their respective fractional covers, of the end-member values. Therefore, when the sensitivity of the NDVI to precipitation is plotted against mean NDVI, an envelope of the data should define the end-member coordinates. We allow the data to define the end members, rather than use training sets of known cover type. The approach taken here requires the conceptual theory of distinctly different water-related dynamics for the cover components to hold true in order to yield reasonable and accurate end members. Therefore, we included only the data for the pixels that have a significant ($P<.1$) sensitivity and we used a constrained optimization technique to construct a triangle that surrounded 99% of the points while minimizing the area of the triangle. The coordinates of the vertices of the triangle were consequently taken as end members (i.e., $\overline{\alpha_j}$ and β_j) for the unmixing model.

2.4. Fractional cover determined for individual years

The unmixing model determines, at each position along the transect, the fixed fractional cover of trees, bare soil only, and grass/bare soil areas. However, while $\langle x_j(i)\rangle$ remain fixed over the 16-year period, the actual fractional cover of the bare soil and grass components fluctuate significantly on an annual basis in response to the wet season rainfall amounts. The bare soil fractional cover for a particular year, x_b, is equal to the sum of $x_{b,only}$ and x_{btrans}. The grass fractional cover, x_g, is then equal to x_{gtrans}. In order to partition $x_{g/b}$ into x_{gtrans} and x_{btrans}, the NDVI value for grass, $\overline{\alpha_g}$, must first be known. This may be inferred from the fixed fractional-cover results, annual rainfall amounts, end-member values, and observed NDVI data. For individual

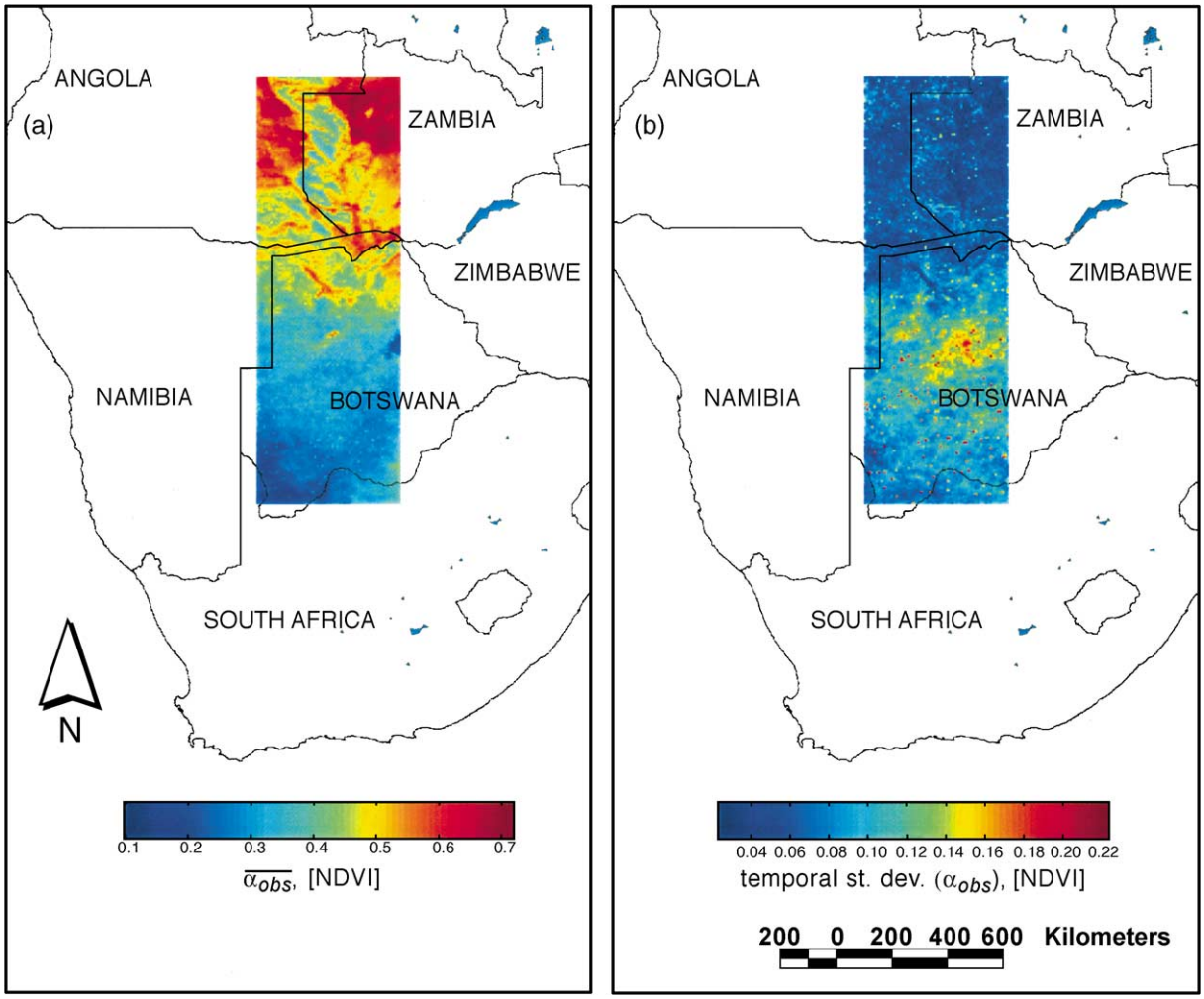

Fig. 2. (a) Mean and (b) temporal standard deviation of the AVHRR-NDVI fields (1983–1998) for the Kalahari Transect (KT). Wet season for NDVI is taken as January–March.

wet seasons, the NDVI for the three fixed-cover types may be expressed as:

$$\langle \alpha_j(i) \rangle = \overline{\alpha_j} + \langle \hat{r}(i) \rangle \beta_j. \tag{6}$$

With the wet-season-specific NDVI for trees and bare soil along the transect determined in this manner, and with the fixed fractional-cover areas known, the remaining NDVI that must be associated with the grass/bare soil area during a particular wet season can be found by inserting the spatially averaged (6) into a non-time-averaged, transformed version of (2):

$$\langle \alpha_{\text{remain}}(i) \rangle = \frac{\langle \alpha_{\text{obs}}(i) \rangle - \langle \alpha_{\text{t}}(i) \rangle \langle x_{\text{t}}(i) \rangle - \langle \alpha_{\text{b,only}}(i) \rangle \langle x_{\text{b,only}}(i) \rangle}{\langle x_{\text{g/b}}(i) \rangle} - \phi_{\text{s}} \tag{7}$$

where $\langle \alpha_{\text{obs}}(i) \rangle$ is the remotely sensed NDVI that is spatially averaged over latitudinal position i for a particular wet season and ϕ_{s} is a correction factor that is applied to the whole of the transect and accounts for sensor- and atmospheric-related temporal variability. This factor is estimated on an annual basis as the mean departures of α_{obs} for a given year from the significant, regressed α_{obs}–$\hat{r}$ linear relationships. The theoretical lower limit to $\langle \alpha_{\text{remain}}(i) \rangle$ for the entire suite of wet seasons is approximately $\overline{\alpha_{\text{b,only}}}$, the NDVI for bare soil. The upper limit of $\langle \alpha_{\text{remain}}(i) \rangle$, which occurs during a very wet year and represents a case in which grass covers the entire area $x_{\text{g/b}}$, is considered to be the NDVI for grass. The upper bound of $\langle \alpha_{\text{remain}}(i) \rangle$ for the suite of wet season rainfall amounts is therefore assigned as $\overline{\alpha_{\text{g}}}$.

With $\overline{\alpha_{\text{g}}}$ inferred in this manner, the fractional-cover components $\langle x_{\text{g}}(i) \rangle$ and $\langle x_{\text{b}}(i) \rangle$ can be calculated for specific wet season rainfall amounts by:

$$\langle x_{\text{b}}(i) \rangle = \langle x_{\text{b,only}}(i) \rangle + \langle x_{\text{btrans}}(i) \rangle = \langle x_{\text{b,only}}(i) \rangle + \langle x_{\text{g/b}}(i) \rangle \left(\frac{\alpha_{\text{g}} - \langle \alpha_{\text{g/b}}(i) \rangle}{\alpha_{\text{g}} - \langle \alpha_{\text{b,only}}(i) \rangle} \right) \tag{8a}$$

and

$$\langle x_g(i)\rangle = \langle x_{gtrans}(i)\rangle = \langle x_{g/b}(i)\rangle \left(\frac{\langle \alpha_{g/b}(i)\rangle - \langle \alpha_{b,only}(i)\rangle}{\alpha_g - \langle \alpha_{b,only}(i)\rangle}\right) \quad (8b)$$

In both equations, the fractional area $\langle x_{g/b}(i)\rangle$ is multiplied by a coefficient ranging between 0 and 1. This coefficient reflects the relative position of the rainfall-specific $\langle \alpha_{g/b}(i)\rangle$ between the NDVI end members of bare soil, $\langle \alpha_{b,only}(i)\rangle$, and grass, $\overline{\alpha_g}$. For the extreme cases in which $\langle \alpha_{g/b}(i)\rangle < \langle \alpha_{b,only}(i)\rangle$ or $\langle \alpha_{g/b}(i)\rangle > \langle \alpha_g(i)\rangle$, the area $\langle x_{g/b}(i)\rangle$ is assigned as entirely bare soil or entirely grass, respectively.

3. Results

Fields of the 16-year wet season mean and interannual standard deviation of NDVI are shown in Fig. 2a and b, respectively. The mean NDVI shows a clear, general decrease from north to south over the KT. The standard deviation in the NDVI peaks near the middle of the transect, bounded by areas of lesser interannual fluctuation in the green biomass cover to the north and south. The slightly speckled appearance of the standard deviation field is caused by AVHRR sensor noise that was introduced at some of the pixel locations during the 1992 wet season.

The mean and temporal standard deviation of wet season precipitation are shown in Fig. 3a and b, respectively. A well-defined north–south mean precipitation gradient is apparent based on the 16 years of data. The pattern displayed by the mean rainfall field is similar to that for the NDVI (Fig. 2a). This similarity does not hold for the standard deviation fields, however. The high temporal standard deviation in seasonal rainfall found in the northern half of the transect is not colocated with the high interannual variability in NDVI located in central Botswana (Fig. 2b). It is evident based on this qualitative comparison that the mean annual rainfall is highly related to the amount to green biomass (as measured by NDVI) along the KT, while the interannual variation in the green biomass is not solely

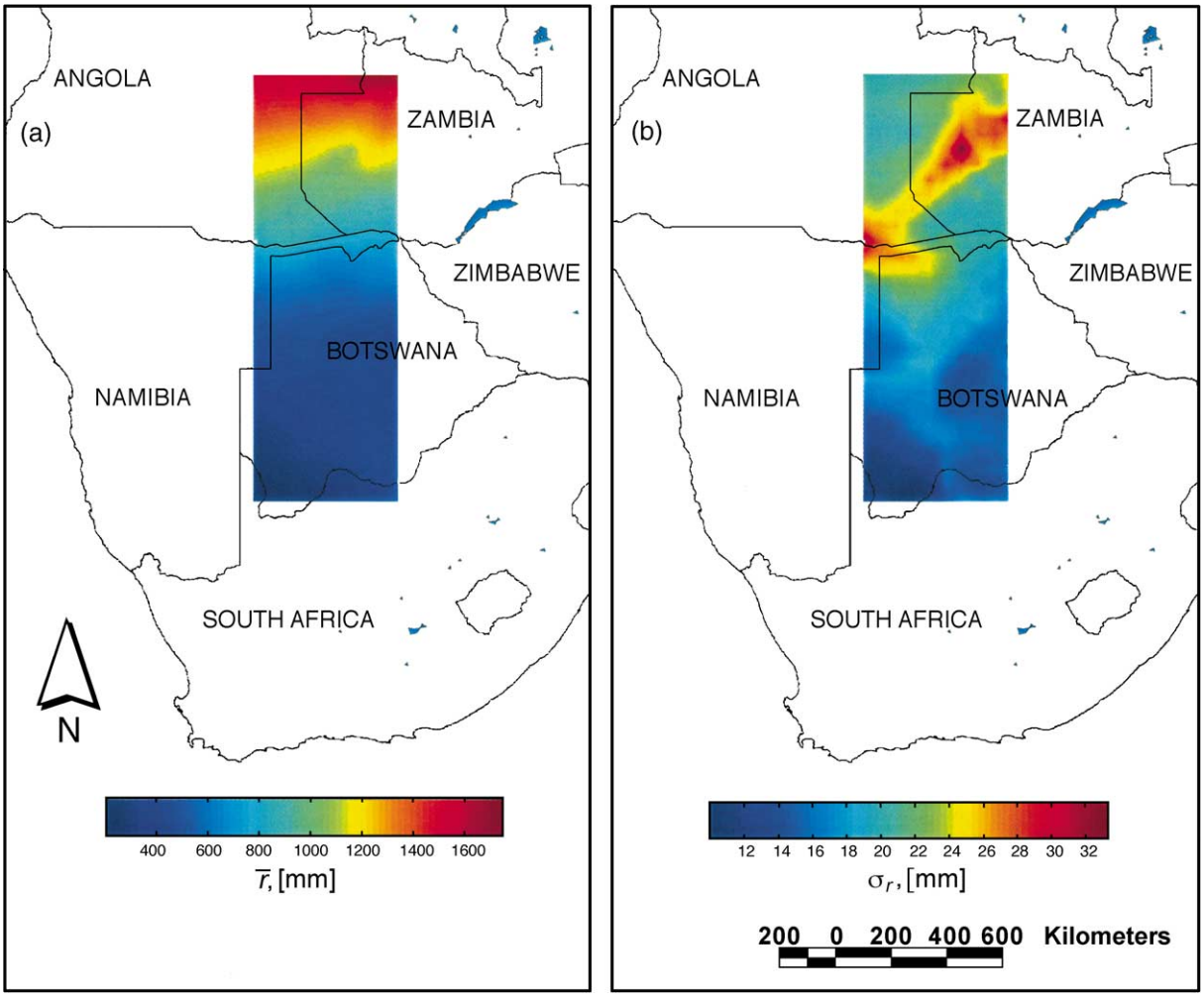

Fig. 3. (a) Mean and (b) temporal standard deviation of the rainfall fields (1983–1998) for the KT. Wet season for rainfall is taken as November–March.

controlled by interannual variability in rainfall. Instead, the vegetation composition plays an important role in determining the extent of the high-frequency variability in NDVI.

Sensitivity of NDVI to precipitation, β_{obs}, at each pixel was evaluated by determining the slope of the best-fit line between the yearly NDVI values and the corresponding normalized precipitation. Fig. 4 shows the sensitivity for all of the pixels with significant ($P<.1$) rainfall–NDVI relationships. Of the initial pixels, 55.7% met this selection criterion for significance, a large proportion considering the relatively rough (0.5°) resolution of the original rainfall data. This represents a 22% improvement on the number of significant relationships yielded by a linear fit between the annual NDVI values and the nonnormalized wet season rainfall totals. Like the temporal variance in NDVI, the peak in the NDVI sensitivity to rainfall is located in the interior of Botswana where annual rainfall is moderate. The cross-sectional averages of these sensitivities, $\langle\beta_{obs}(i)\rangle$, are used as input for the unmixing model along with the spatial average of the temporal mean NDVI field, $\langle\overline{\alpha_{obs}}(i)\rangle$. These profiles along the KT are shown in Fig. 5.

The coefficients $\overline{\alpha_j}$ and β_j, used in Eqs. (2) and (3), respectively, are determined from the scatter plot of β_{obs} versus $\overline{\alpha_{obs}}$ (Fig. 6). This plot consists of the β_{obs} values shown in Fig. 4 as a function of their corresponding mean NDVI values, $\overline{\alpha_{obs}}$. Only points having a significant relationship between wet season NDVI and wet season rainfall were used. Three different cover types were originally assumed to represent the land surface and, indeed, the data do fall in a pattern that supports this a priori assumption of linear mixing with three end members. Specific values for the end members were assigned as the coordinates of the

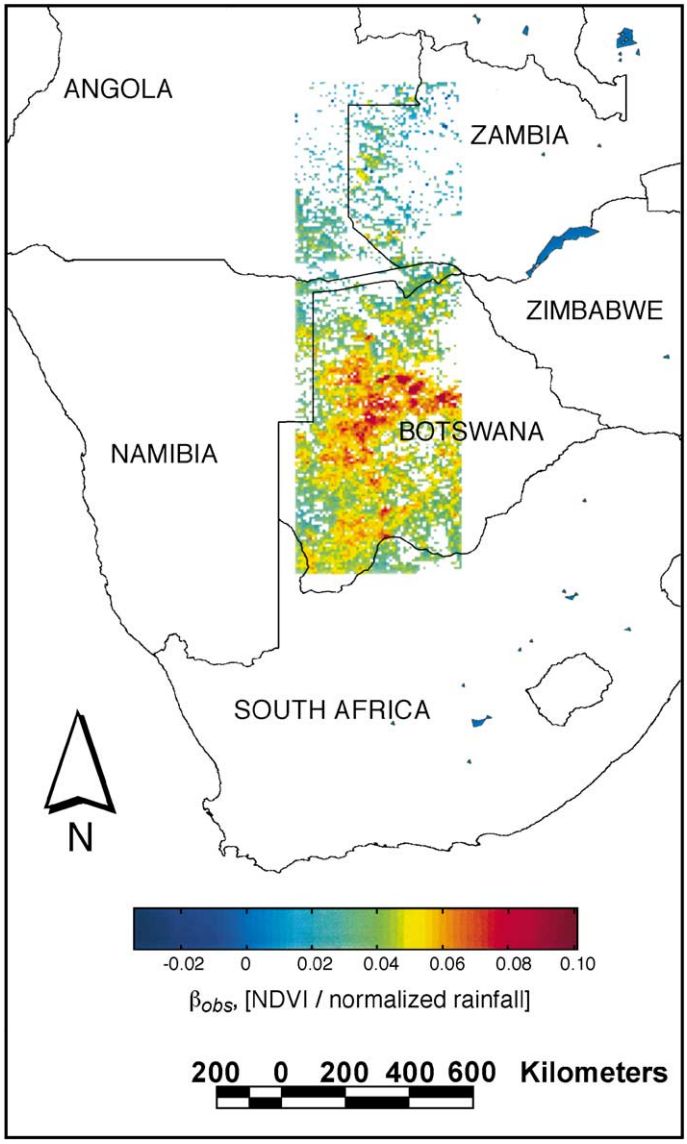

Fig. 4. Slope in the relationship between wet season NDVI and normalized wet season rainfall for each pixel, β_{obs}. Only those pixels having a significant ($P<0.1$) relationship are shown.

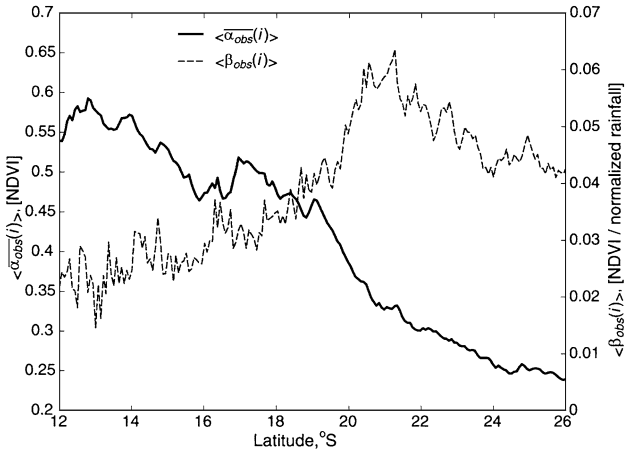

Fig. 5. Latitudinal averages of mean NDVI, $\langle\overline{\alpha_{\mathrm{obs}}}(i)\rangle$, and sensitivity of NDVI to rainfall, $\langle\beta_{\mathrm{obs}}(i)\rangle$, along the transect, used as input to the linear unmixing model.

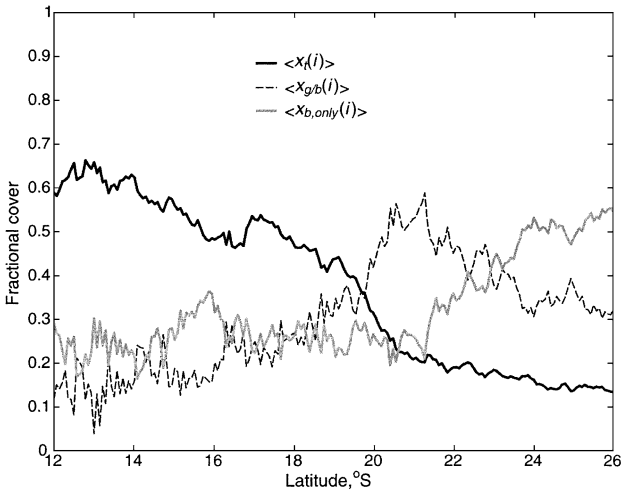

Fig. 7. Results of the linear unmixing model using the long-term NDVI and rainfall data.

triangle vertices that bound the data. These vertices were categorized on the basis of the qualitative characteristics of tree, bare soil, and transient grass areas. Trees, which have multiple levels of green foliage, deep roots, and a relatively stable deep water supply, are associated with a mean wet season NDVI of 0.82 and a low sensitivity to interannual variations in precipitation of 0.008 units NDVI/normalized rainfall. Bare soil has a minimal mean NDVI of 0.09 and has a slightly higher sensitivity to precipitation of 0.018. This slight NDVI increase for wetter soils is in agreement with prior findings that this index increases with decreasing soil brightness for constant vegetation cover (Huete, Jackson, & Post, 1985; Huete & Tucker, 1991). Finally, the transient grass/bare soil area has a moderate mean NDVI of 0.25 and is highly sensitive to interannual variations in precipitation, with a value of 0.099 for $\beta_{\mathrm{g/b}}$. These coefficients taken from the vertices of the triangle are then used in the linear unmixing procedure.

The unmixing results for the KT shown in Fig. 7 indicate decreasing tree fractional cover along the north–south mean annual rainfall gradient. The area that is persistently bare soil remains relatively level for the northern two-thirds of the transect and then increases over the most arid region to the south. Finally, the transient grass/ bare soil area, $\langle x_{\mathrm{g/b}}(i)\rangle$, peaks between 22° and 23°S latitude, corresponding to a tree fractional cover of about 22%.

Fractional-cover estimation on a yearly basis requires the determination of the NDVI end member for grass, $\overline{\alpha_{\mathrm{g}}}$, which was achieved by plotting the results of Eq. (7) for each of the 16 years (Fig. 8). The correction factor in Eq. (7) was small for each of these years, in the range $-0.064<\phi_{\mathrm{s}}<0.081$. Theoretically, the lower range of

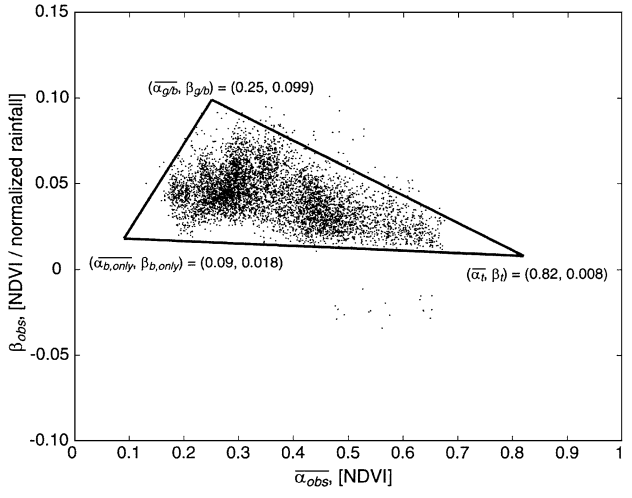

Fig. 6. Scatter plot of $\overline{\alpha_{\mathrm{obs}}}$ and β_{obs} for all of the pixels having a significant ($P<0.1$) relationship for β_{obs} (those shown in Fig. 4). The triangle is fit to minimize the area while retaining 99% of the data within its bounds. End-member values for the linear unmixing model are taken as the coordinates of the vertices of the triangle.

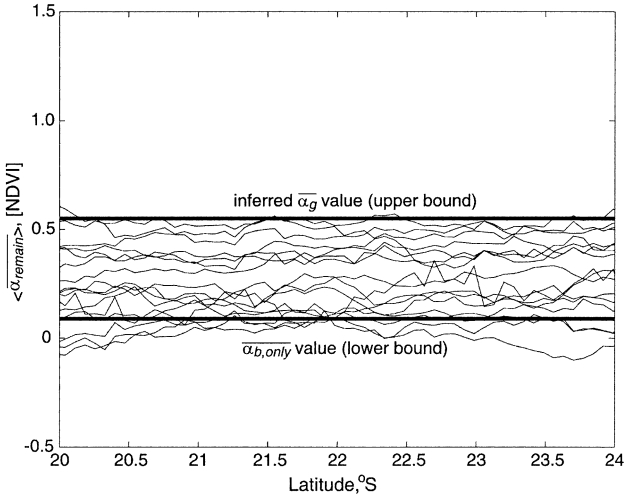

Fig. 8. Plots of $\langle\overline{\alpha_{\mathrm{remain}}}(i)\rangle$ for the 16 years along a portion of the transect. The mean NDVI for grass, $\overline{\alpha_{\mathrm{g}}}$, is estimated from the upper bound.

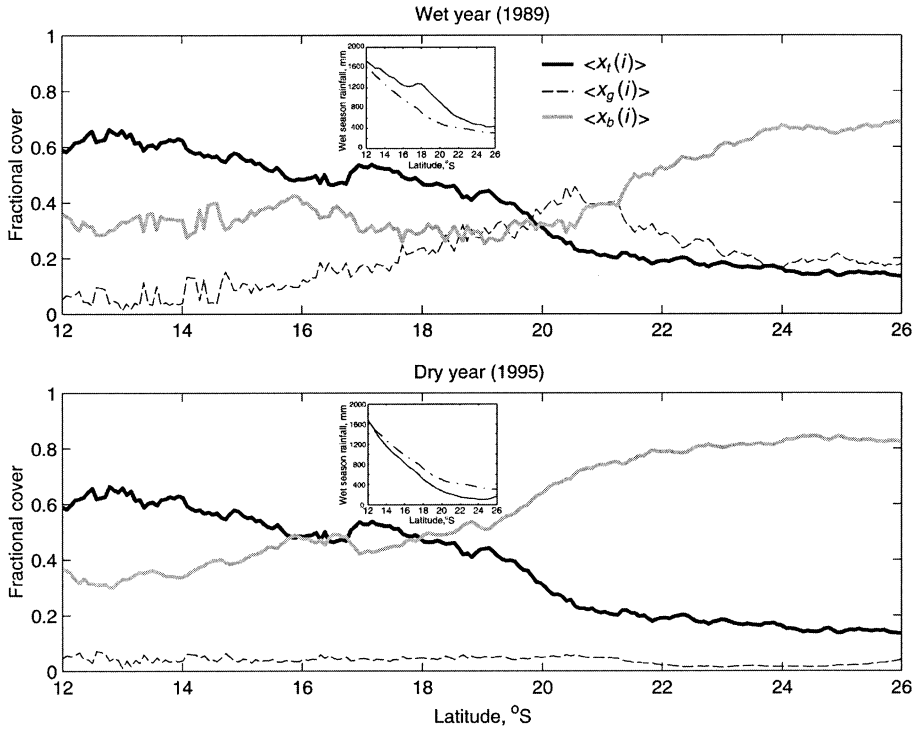

Fig. 9. Comparison of fractional-cover components for a wet year (top) and a dry year (bottom). Insets show the rainfall along the transect for the particular wet season (solid line) in relation to the wet season mean (dashed line).

$\langle \alpha_{\text{remain}}(i) \rangle$ should be approximately $\overline{\alpha_{\text{b,only}}}$ during dry years when there is very little grass, and the upper range should be $\overline{\alpha_{\text{g}}}$, during wet years when grass covers the entirety of this area. Fig. 8 shows the results for the suite of years, covering the latitudes 20–24°S, where $\langle x_{\text{g/b}}(i) \rangle$ is relatively large. Elsewhere on the transect, the smaller $x_{\text{g/b}}$ causes amplification in any sensor noise that may be associated with the calculation of $\langle \alpha_{\text{remain}}(i) \rangle$ from Eq. (7). This figure shows remarkably level lines along the selected portion of the transect for the individual years, with the $\langle \alpha_{\text{remain}}(i) \rangle$ levels representing the composite NDVI for the transient grass/bare soil area. The upper bound, estimated at 0.55, is assigned as the NDVI for the grass.

With $\overline{\alpha_{\text{g}}}$ identified, fractional-cover amounts were estimated for sample wet and dry years, as shown in Fig. 9. For a wet year, 1989, in which the rainfall was greater than the mean at each latitudinal position along the transect (see inset), the grass cover approaches its potential area, $\langle x_{\text{g/b}}(i) \rangle$. In the case of a dry year, 1995, the grass cover is very low at all positions along the transect, resulting in an expansion of the bare soil cover.

4. Discussion

Although potential limitations associated with the analysis of multiyear AVHRR-NDVI data have been recognized (e.g., DeFries et al., 2000), the long-term temporal aspect of the data can be extremely beneficial for extracting information about land-cover processes in water-limited environments when carefully analyzed. Rather than basing our analysis on relative differences in NDVI between years, which would be problematic due to shifts in sensor-related instead of vegetation-related factors, we use the long-term mean NDVI and the sensitivity of the NDVI with respect to an independently collected variable, rainfall, as input to the model. Hence, only temporal variability in NDVI tied to precipitation affect the results. The method presented here for fractional-cover derivation is based upon fundamental vegetation processes, rather than on empirically derived correlations. Training sets and calibration procedures are not needed. Furthermore, this method allows for future predictions of total NDVI and fractional cover along the transect, using rainfall as input, that are based solely upon previous satellite and rainfall observations.

Previous studies have found the relationship between interannual variations in rainfall and NDVI to be weak in southern Africa, except for in the moderately dry areas (Goward & Prince, 1995; Richard & Poccard, 1998). In the analysis presented here, we first had to define the temporal and functional attributes of the interannual rainfall–NDVI relationship, since no consistent methodology currently exists. We chose to focus on the wet season, limiting the window to the time of the year when the vegetation is near its peak and is effected by the antecedent rainfall amounts. We found that using normalized rainfall in the rainfall–NDVI relationship improved the number of pixels meeting the significance criterion, since this appro-

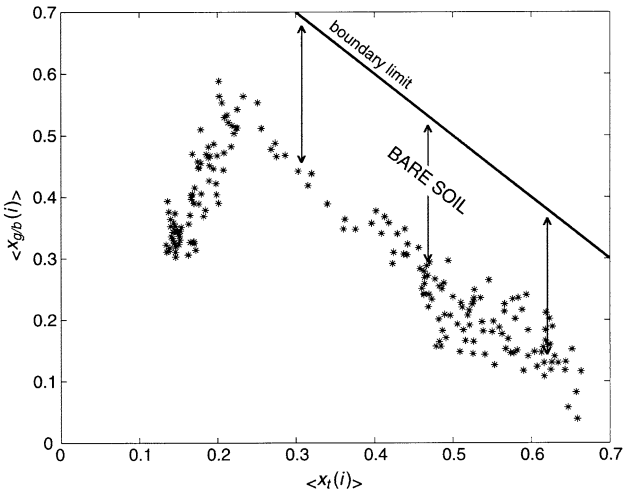

Fig. 10. Fractional potential grass cover, $\langle x_{g/b}(i)\rangle$, as a function of fractional tree cover, $\langle x_t(i)\rangle$. Bare soil cover is largely constant on the wetter end of the transect, making up the difference between the potential grass cover and its theoretical upper limit.

priately limits the weight of extreme rainfall anomalies. The majority of wet season rainfall in this region comes in the form of short-lived convective storms. Above a certain threshold, storm precipitation can exceed the amount that can be of use for augmented grass growth. On the other extreme, the retreat of the grass cover during drought years is somewhat attenuated by the presence of residual soil moisture. The strongest correlations exist within Botswana, where the slope in the rainfall–NDVI relationship is greatest. This slope, or sensitivity, decreases on the northern end of the transect where the mean annual precipitation is higher (Fig. 4) and tree shading may limit grass potential. The low density of points having significant relationships in the northern end of the transect may be attributable to the decreased signal-to-noise ratio of the data here. Temporal variations in sensor-related factors can drown out any subtle rainfall–NDVI relationships that may be present in this northern region where NDVI does not vary much from year to year. For these tree-dominated regions, there may be a more suitable alternative to the significance criterion presented here.

The geometric outline of the data for β_{obs} as a function of $\overline{\alpha_{obs}}$ (Fig. 6) suggests three vertices, and the cover types that the end members represent are readily apparent. The transient grass/bare soil area has by far the highest sensitivity to NDVI, but has a mean NDVI that is closer to that of bare soil than trees. This is due in part to the actual grass cover area being, on average, a fraction of area $x_{g/b}$. Ideally, the positions of the end members would be orthogonal in order to facilitate linear mixing with the least amount of uncertainty. From the position of the end members, it is apparent that mean NDVI along the transect will largely control the fractional cover of trees and the sensitivity to rainfall will largely control the extent of the potential grass area. Indeed, this is the case with an R^2=.99 for the former relationship and an R^2=.90 for the latter. While these correlations may be high, the absolute amounts of the fractional-cover areas are controlled by the end-member positions. Percent cover along the transect shows an expected decrease in trees, but the potential grass area, $\langle x_{g/b}(i)\rangle$, peaks where the mean wet season precipitation is between 400 and 500 mm (Fig. 7).

Another way to examine the unmixing results is to consider the relationship between the fractional tree cover and the fractional potential grass cover. Fig. 10 shows that the potential grass area sharply peaks when the tree cover is approximately 22%. It appears that above approximately 450 mm of mean wet season precipitation, the maximum extent of the grass cover is limited by the tree cover, while below this threshold the maximum extent of the grass cover is limited by the mean wet season precipitation. The fractional tree cover over the KT is highly related to the mean wet season precipitation (R^2=.87). The persistent bare soil area is remarkably constant over the wetter portion of the transect, suggesting an upper threshold on the percentage of the land surface that can be cover by vegetation in this tree-dominated portion of the savanna system.

Ground measurements of fractional tree cover taken at a number of locations along the KT (Scholes, Dowty, Caylor, Parsons, & Shugart, in press), can be compared with the unmixing model results. Most of the field sites were selected on the basis of being representative of the immediate surrounding area, as judged from high resolution satellite images. Fractional cover was derived by sampling methods for tree individuals. When compared with the modeled fractional cover, it is evident that the analysis framework captures the decline in tree cover from north to south along the transect (Fig. 11). The most significant departures are apparent on the northern end of the transect, which could be the result of cross-sectional averaging over latitudinal positions in the unmixing method, whereas the field measurements were taken at points. For instance, the northernmost

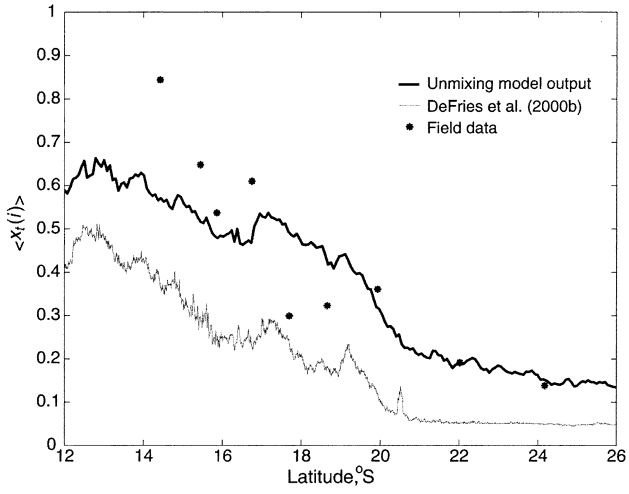

Fig. 11. Model results for fractional tree cover, $\langle x_t(i)\rangle$, compared with field data measured at positions along the KT. Fractional tree cover from DeFries, Hansen, Townshend, Janetos, and Loveland (2000) is also shown.

field measurement, which has a much higher fractional tree cover than the model-predicted value for this latitude, was taken from an area to the east of the Zambezi flood plain that has a higher NDVI than the cross-sectional average at this latitude (see Fig. 2). This field location was unlike the other sites in that it was selected on the basis of representing a nearly closed canopy (R. Scholes, pers. comm.). An independently derived fractional tree cover estimate is shown on the graph as well from DeFries et al. (2000). These data were taken from a global tree cover product so comparison with the regional analysis is perhaps incongruent. However, there is a noticeable offset between the two methods along the transect. As for grass cover, model validation with respect to predictions of this component is difficult due to its transient nature.

The method for determining fractional cover presented here assumes that there are no shifts in tree density distribution or land conversion along the transect over the 16-year period. The low population density of the Kalahari region limits the potential of anthropogenic vegetation disturbance, but some deforestation or grazing effects likely have resulted in localized land cover changes during this time. Since the focus of this paper is the regional climate–vegetation interaction, we average over latitudinal bands along the transect in order to avoid impact from some of these smaller-scale factors. Although woody vegetation encroachment has been documented in a savanna systems over a period of several decades due to long term shifts in precipitation, such as in Texas (Archer, Scifres, Bassham, & Maggio, 1988), we assume that this has not occurred on a large scale for the KT during the time in which the remote sensing data were collected. No general trends in regional rainfall amounts were observed to have occurred during the 16-year period. The unmixing method presented here provides estimates of fixed areas that are either steady (x_t and $x_{b,only}$) or transient ($x_{g/b}$) in composition, but this method also allows for yearly estimates of the fractional cover based upon rainfall (Fig. 9). The ability to make fractional-cover predictions for future rainfall scenarios from past observations provides a unique advantage over traditional unmixing models.

Goward and Prince (1995), based upon time series of NDVI and rainfall data in southern Africa, suggest that the there is some "memory" in the system from prior years such that the NDVI response of a particular year is influenced by the rainfall in the previous year. This is an interesting concept that can be applied to the model framework presented in this paper. The derived cover areas, $\langle x_t(i)\rangle$, $\langle x_{b,only}(i)\rangle$, and $\langle x_{g/b}(i)\rangle$, along the KT can be thought of as a matrix that converts an input of rainfall along the transect into a wet season-specific output of $\langle x_t(i)\rangle$, $\langle x_b(i)\rangle$, and $\langle x_g(i)\rangle$. If there is indeed some memory in the system, this memory may be a direct function of the tree, grass, and bare soil cover from the previous year. For this conceptualization, as shown in Fig. 12, the vegetation cover yielded by a wet season rainfall scenario would alter the matrix,

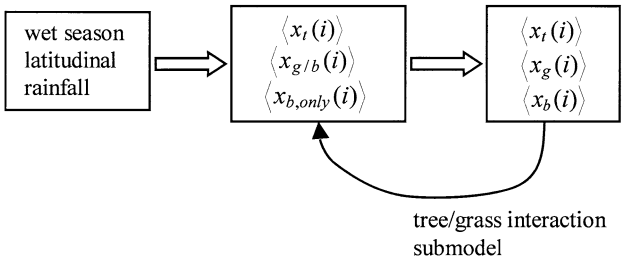

Fig. 12. Schematic diagram showing the interface of the remote sensing results with a tree/grass interaction model to predict future surface cover in response to climate variability.

which would in turn affect the next year's vegetation cover. For a simple conceptualization, the memory for grass could be physically represented by seed dispersal. Following a wet season with above average rainfall, the grass cover area may be more sensitive to rainfall due to the presence of more widely distributed seeds, which would be represented in the model by $\langle x_{g/b}(i)\rangle$ gaining size at the "expense" of $\langle x_{b,only}(i)\rangle$. Lower frequency alterations, such as shifts in fractional tree cover, could be represented by slight increases or decreases in $\langle x_t(i)\rangle$ at the expense of $\langle x_{g/b}(i)\rangle$, in response to rainfall anomalies relative to the mean wet season rainfall needed for a stable $\langle x_t(i)\rangle$. Parameter-intensive methods have been developed to describe localized tree–grass coexistence in savanna systems (Rodriguez-Iturbe et al., 1999a, 1999b); however, there is justifiable need for the development of lower-dimensional models that rely on some of the larger-scale relationships between fractional cover and rainfall that can be observed via remote sensing.

5. Conclusions

There currently exists the need to establish estimates of fractional surface cover over large geographical areas for use in fuel load models of biomass burning as well as in land–atmosphere exchange models. In both cases, the compositional mixture of trees and grass plays a major role in defining the function of the system. Reliable multiyear estimates of fractional cover in savannas have proven to be elusive, however. Additionally, large-scale linkages between rainfall and vegetation cover dynamics have yet to be satisfactorily explored. In this paper, we developed and presented a framework for merging time series of remotely sensed NDVI and ground-measured rainfall to estimate fractional cover based upon the disparate growth characteristics of trees and grass in response to interannual variability in rainfall in a water-limited system. An unmixing procedure was introduced that relies upon quantifying the temporal mean NDVI and the sensitivity of NDVI to interannual variations in rainfall for individual cover components. The derivation of end members for the unmixing model rested upon—and supported—the validity of the conceptual theory

of distinctly different water-related dynamics for these components.

This represents an alternative to traditional methods for finding fractional cover, which often involve the use of training sets in the spectral unmixing of empirically derived metrics. Year-to-year variations in atmospheric and sensor-related factors can limit the potential applicability of traditional unmixing methods to single-year time frames since recalibration can induce spurious differences in inferred cover composition between years. The method presented here uses long-term data that isolates the response of NDVI to variations in rainfall, and by doing so fractional-cover estimates for specific years can be generated. No a priori information is used as input to the model. Predictions of fractional cover in response to future rainfall scenarios can also be formed on this basis, although long-term predictions must include dynamic alterations in the values of $\langle x_t(i)\rangle$, $\langle x_{b,only}(i)\rangle$, and $\langle x_{g/b}(i)\rangle$. This could account for the effects of woody vegetation encroachment or recession, which were assumed to be negligible on a regional scale over the 16-year period of analysis.

We used the KT in southern Africa as a site to apply the rainfall–NDVI unmixing method. We found a strong relationship between fractional tree cover and mean wet season precipitation along the transect (R^2=.87). Potential grass cover peaked at approximately 450 mm of mean wet season precipitation. Above this value, the potential grass area was found to be controlled by the tree cover. Below 450 mm, the potential grass area appeared to be limited by the available rainfall. Estimates of actual tree, grass, and bare soil fractional cover for individual wet seasons were also generated by this method, illustrating the dynamic conversion between bare soil and grass areas as a result of differing rainfall in wet and dry years. Although we focus our analysis on this particular regional setting, the applicability of this method to savannas in general looks to be promising.

Acknowledgements

Funding for this research was provided by a NASA New Investigator Program in the Earth Sciences award (NAG5-8670). The authors appreciate the thoughtful discussion and input by Tim Newman. We also thank the three anonymous reviewers for their comments on an earlier version of this paper. Data used by the authors in this study include data produced through funding from the Earth Observing System Pathfinder Program of NASA's Mission to Planet Earth in cooperation with the National Oceanic and Atmospheric Administration. The data were provided by the Earth Observing System Data and Information System (EOSDIS), Distributed Active Archive Center at Goddard Space Flight Center, which archives, manages and distributes this data set. Precipitation data were provided by David Viner of the Climate Impacts LINK Project, Climate Research Unit, University of East Anglia.

References

Agbu, P. A., & James, M. E. (1994). The NOAA/NASA Pathfinder AVHRR land data set user's manual. Greenbelt, MD: Goddard Distributed Active Archive Center Publications, GCDG.

Archer, S., Scifres, C., Bassham, C. R., & Maggio, R. (1988). Autogenic succession in a subtropical savanna: conversion of grassland to thorn woodland. *Ecological Monographs*, *58*, 111–127.

Bateson, A., & Curtiss, B. (1996). A method for manual endmember selection and spectral unmixing. *Remote Sensing of Environment*, *55*, 229–243.

Belsky, A. J. (1994). Influences of trees on savanna productivity: tests of shade, nutrients, and tree–grass competition. *Ecology*, *75*(4), 922–932.

Burgess, T. L. (1995). Dessert grassland, mixed shrub savanna, shrub steppe, or semidesert scrub? The dilemma of coexisting growth forms. In M. P. McClaran, & T. R. Van Devender (Eds.), *The desert grassland* (pp. 31–67). Tucson, AZ: The University of Arizona Press.

Dean, W. R., Milton, S. J., & Jeltsch, F. (1999). Large trees, fertile islands, and birds in arid savanna. *Journal of Arid Environments*, *41*(1), 61–78.

DeFries, R. S., Hansen, M. C., & Townshend, J. R. G. (2000). Global continuous fields of vegetation characteristics: a linear mixture applied to multi-year 8 km AVHRR data. *International Journal of Remote Sensing*, *21*(6 and 7), 1389–1414.

DeFries, R. S., Hansen, M. C., Townshend, J. R. G., Janetos, A. C., & Loveland, T. R. (2000). A new global 1-km dataset of percentage tree cover derived from remote sensing. *Global Change Biology*, *6*(2), 247–254.

Doergeloh, G. W. (2000). Relative densities and habitat utilization of non-utilized, terrestrial gamebird populations in a natural savanna, South Africa. *African Journal of Ecology*, *38*(1), 31–37.

Ehleringer, J. R., & Monson, R. K. (1993). Evolutionary and ecological aspects of photosynthetic pathway variation. *Annual Review of Ecology and Systematics*, *24*, 411–439.

Eischeid, J. K., Diaz, H. F., Bradley, R. S., & Jones, P. D. (1991). *A comprehensive precipitation data set for global land areas*, US Department of Energy Report No. DOE/ER-69017T-H1, Washington, DC, 81 pp.

Farrar, T. J., Nicholson, S. E., & Lare, A. R. (1994). The influence of soil type on the relationships between NDVI, rainfall, and soil moisture in semiarid Botswana: II. NDVI response to soil moisture. *Remote Sensing of Environment*, *50*, 121–133.

Frost, P. G. H. (1984). Organic matter and nutrient dynamics in a broad-leafed African savanna. In J. C. Tothill, & J. J. Mott (Eds.), *Ecology and management of the world's Savannas. International Savanna symposium 1984* (pp. 200–206). Brisbane, Australia: Austrailian Academy of Sciences.

Fuller, D. O. (1994). *Foliar phenology of savanna vegetation in south-central Africa and its relevance related to climate change.* PhD dissertation, University of Maryland, College Park, Maryland.

Fuller, D. O., & Prince, S. D. (1996). Rainfall and foliar dynamics in tropical southern Africa: potential impacts of global climatic change on savanna vegetation. *Climatic Change*, *33*, 69–96.

Goward, S. M., & Prince, S. D. (1995). Transient effects of climate on vegetation dynamics: satellite observations. *Journal of Biogeography*, *22*, 549–563.

Grist, J., Nicholson, S. E., & Mpolokang, A. (1997). On the use of NDVI for estimating rainfall fields in the Kalahari of Botswana. *Journal of Arid Environments*, *35*, 195–214.

Guenther, A. B., Zimmerman, O. L. P., Greenberg, J., Scholes, R., & Scholes, M. (1996). Biogenic hydrocarbon emissions from southern African savannas. *Journal of Geophysical Research*, *101*(D20), 25859–25865.

Hanan, N. P., Prince, S. D., & Hiernaux, P. H. Y. (1991). Spectral modelling of multicomponent landscapes in the Sahel. *International Journal of Remote Sensing*, *12*(6), 1243–1258.

Hoffa, E. A., Ward, D. E., Hao, W. M., Susott, R. A., & Wakimoto, R. H. (1999). Seasonality of carbon emissions from biomass burning in a Zambian savanna. *Journal of Geophysical Research*, *104*(D11), 13841–13853.

Huete, A. R., Jackson, R. D., & Post, D. F. (1985). Spectral response of a plant canopy with different soil backgrounds. *Remote Sensing of Environment*, *17*, 37–53.

Huete, A. R., & Tucker, C. J. (1991). Investigation of soil influences in AVHRR red and near-IR vegetation index imagery. *International Journal of Remote Sensing*, *12*, 1223–1242.

Hulme, M. (1992a). Rainfall changes in Africa: 1931–1960 to 1961–1990. *International Journal of Remote Sensing*, *12*, 685–699.

Hulme, M. (1992b). A 1951–80 global land precipitation climatology for the evaluation of general circulation models. *Climate Dynamics*, *7*, 57–72.

James, M. E., & Kalluri, S. N. V. (1994). The Pathfinder AVHRR land data set: an improved coarse resolution data set for terrestrial monitoring. *International Journal of Remote Sensing*, *15*, 3347–3364.

Kerdiles, H., & Grondona, M. O. (1995). NOAA-AVHRR NDVI decomposition and subpixel classification using linear mixing in the Argentinean Pampa. *International Journal of Remote Sensing*, *16*, 1303–1325.

Koch, G. W., Scholes, R. J., Steffen, W. L., Vitousek, P. M., & Walker, B. H. (1995). *The IGBP terrestrial transects: Science plan*, Report No. 36, Stockholm: International Geosphere-Biosphere Programme, 61 pp.

Myneni, R. B., Maggion, S., Jaquinta, J., Privette, J. L., Gordon, N., Pinty, B., Kimes, D. S., Verstraete, M. M., & Williams, D. L. (1995). Optical remote sensing of vegetation: modeling, caveats, and algorithms. *Remote Sensing of Environment*, *51*(1), 169–188.

New, M., Hulme, M., & Jones, P. (1999). Representing twentieth-century space–time climate variability: Part I. Development of a 1961–1990 mean monthly terrestrial climatology. *Journal of Climate*, *12*(3), 829–856.

Nicholson, S. E., & Farrar, T. J. (1994). The influence of soil type on the relationships between NDVI, rainfall, and soil moisture in semiarid Botswana: I. NDVI response to rainfall. *Remote Sensing of Environment*, *50*, 107–120.

Palmer, A. R., & van Rooyen, A. F. (1998). Detecting vegetation change in the southern Kalahari using Landsat TM data. *Journal of Arid Environments*, *39*, 143–153.

Richard, Y., & Poccard, I. (1998). A statistical study of NDVI sensitivity to seasonal and interannual rainfall variations in southern Africa. *International Journal of Remote Sensing*, *19*(15), 2907–2920.

Roberts, D. A., Smith, M. O., & Adams, J. B. (1993). Green vegetation, nonphotosynthetic vegetation, and soils in AVHIRIS data. *Remote Sensing of Environment*, *44*, 255–269.

Rodriguez-Iturbe, I., D'Odorico, P., Porporato, A., & Ridolfi, L. (1999a). Tree–grass coexistence in savannas: the role of spatial dynamics and climate fluctuations. *Geophysical Research Letters*, *26*(2), 247–250.

Rodriguez-Iturbe, I., D'Odorico, P., Porporato, A., & Ridolfi, L. (1999b). On the spatial and temporal links between vegetation, climate, and soil moisture. *Water Resources Research*, *35*(12), 3709–3722.

Scanlon, T. M., & Albertson, J. D. (submitted for publication). Canopy scale measurements of CO_2 and water vapor exchange along a precipitation gradient in southern Africa. *Global Change Biology.*

Scholes, R. J., Dowty, P. R., Caylor, K., Parsons, D. A. B., & Shugart, H. H. (in press). Trends in savanna structure and composition on an aridity gradient. *Journal of Vegetation Science.*

Settle, J. J., & Drake, N. A. (1993). Linear mixing and the estimation of ground cover proportions. *International Journal of Remote Sensing*, *14*(6), 1159–1177.

Shea, R. W., Shea, B. W., Kauffman, J. B., Ward, D. E., Haskins, C. I., & Scholes, M. C. (1996). Fuel biomass and combustion factors associated with fires in savanna ecosystems of South Africa and Zambia. *Journal of Geophysical Research*, *101*(D19), 23551–23568.

Smit, G., & Rethman, N. F. G. (2000). The influence of tree thinning on the soil water in a semi-arid savanna of southern Africa. *Journal of Arid Environments*, *44*(1), 41–59.

Smith, M. O., Johnston, P. E., & Adams, J. B. (1985). Quantitative determination of mineral types and abundances from reflectance spectra using principle component analysis. *Journal of Geophysical Research*, *90, 797–804.*

Thomas, D. S. G., & Shaw, P. A. (1993). The evolution and characteristics of the Kalahari, southern Africa. *Journal of Arid Environments*, *25*(1), 97–108.

Van Der Meer, F., & De Jong, S. M. (2000). Improving the results of spectral unmixing of Landsat Thematic Mapper imagery by enhancing the orthogonality of end-members. *International Journal of Remote Sensing*, *21*(15), 2781–2797.